MATERIALS PHYSICS AND MECHANICS RESEARCH ARTICLE

Submitted: August 13, 2024 **Revised: September 8, 2024** **Accepted: September 29, 2024**

Influence of latent heat and heat exchange conditions on tension behavior of shape memory alloy specimen

F.S. Belyaev [1,2], A.E. Volkov [1], E.A.Vukolov [1], M.E. Evard [1] ✉, K.V. Kudrina [1], M.S. Starodubova [1]

[1] St. Petersburg State University, St. Petersburg, Russia

[2] Institute for Problems in Mechanical Engineering of the Russian Academy of Sciences, St. Petersburg, Russia

✉ m.evard@spbu.ru

ABSTRACT

A microstructural model of functional behavior of shape memory alloys has been used for modeling of the pseudo-elasticity effect taking into account the influence of latent heat of the martensitic transformations, heat exchange conditions and strain rate. A completely coupled boundary value problem on tension of a cylindrical rod under conditions of heat exchange with the environment and heat diffusion along the radius has been solved. The obtained results are in good agreement with the available experimental data. The Fourier and Biot criteria were used to evaluate the critical radius, for which it is necessary to solve a fully coupled boundary value problem at given material parameters, deformation rate and heat exchange conditions. It has been shown that the microstructural model taking into account the latent heat release and adsorption is an adequate tool for describing the strain rate dependence of the pseudo-elastic behavior for shape memory alloys.

KEYWORDS

heat exchange conditions • latent heat • microstructural modeling • shape memory alloys • TiNi • tension boundary value problem • Fourier number • Biot number

Acknowledgements. *This work has been supported by the grant of the Russian Science Foundation, RSF 23-21-00167.*

Citation: Belyaev FS, Volkov AE, Vukolov EA, Evard ME, Kudrina KV, Starodubova MS. Influence of latent heat and heat exchange conditions on tension behavior of shape memory alloy specimen. *Materials Physics and Mechanics*. 2024;52(5): 18–28.
http://dx.doi.org/10.18149/MPM.5252024_2

Introduction

Nowadays the ability of shape memory alloy (SMA) parts to restore the original shape at heating after preliminary deformation (shape memory effect), as well as pseudoelastic behavior consisting in the recovery of significant deformations during isothermal unloading, has found wide application. These materials are used as active working elements of actuators and sensors [1,2], passive and semi-active vibration protection devices [3], medical devices [4,5]. The functional properties of SMAs are caused by martensitic transformations - reversible change of the crystal lattice from a high-temperature austenitic structure to a low-temperature martensitic one. Martensitic transformations in SMAs are usually controlled by temperature kinetics, so that the volume fraction of martensite smoothly increases at cooling through the temperature interval of the direct transformation and decreases at heating through the interval of the reverse transformation [6]. The finite rate of heat diffusion and the processes of release (or absorption) of the latent heat of the transformation can have a significant influence

on functional characteristics of a particular device [7–9]. For example, cyclic temperature variations of SMA samples associated with the release and absorption of the latent heat of transformation were revealed during cyclic loading at constant ambient temperature. Moreover, the oscillation amplitude increases with the loading rate [10,11]. Heat exchange with the environment leads to an attenuation of the influence of internal heat sources [12], but sometimes the heat exchange can be difficult, especially when an SMA element has a coating [13,14]. At some conditions, a loaded sample may develop deformation in time due to a delay of the martensitic transformation caused by the presence of two simultaneous processes: the release of the latent heat of transformation and heat flux to the environment [15].

Simulation, which takes into account the presence of internal heat sources in SMA elements and heat exchange conditions becomes especially important for devices that are required to operate at a given temperature and/or within a given time interval. For modelling of SMA element deformation different theoretical approaches can be used. For solving boundary value problems to find the stress and strain fields usually a macroscopic (phenomenological) model is used for calculation of the SMA deformation. In such models the volume fraction of the martensitic phase and the transformation strain are considered as internal variables, and the relationships that determine their evolution are based either directly on the results of experiments [16], or on a combination of experimental constitutive relations with basic thermodynamic principles [17–21]. When it is necessary to describe the reorientation of martensite, phenomenological models either introduce two types of martensite – chaotic and oriented, or consider the existence of several orientational variants or martensite plates and formulate criteria for reorientation [22,23]. Unfortunately, the ability of macroscopic models to describe the entire set of functional properties of SMA at changing thermal and mechanical regimes are greatly limited due to the lack of direct consideration of the structure of martensite and the details of the mechanisms of transformation and reorientation. Microstructural models of the behavior of SMAs [24–26], based on accounting for the structure of these materials and the specific features of the deformation mechanisms, have greater capabilities. Although a large number of internal variables as well as the complexity of determining the material constants are the obstacles for using such models, there are a few successful examples of solving boundary value problems for SMA elements based on a microstructural model [27–29]. In the present work, the simulation of pseudoelastic behavior of an SMA cylinder at different strain rates accounting the influence of heat release/absorption during martensitic transformations as well as heat exchange conditions have been performed. Two approaches within the frames of the microstructural model were used. The first one did not involve solving a boundary value problem in the classical sense and could be considered as a zero-dimensional problem for a cylinder with a uniform temperature field. The second one is the completely coupled boundary value problem. Since solving the connected boundary value problems for SMA bodies is associated with a number of difficulties, a theoretical estimate of the critical radius for the cylinder at which the temperature field can be considered homogeneous at a given loading rate and heat transfer conditions was made. It could reduce the cost of time and computational resources

Microstructural model

The microstructural model used in this work is described in detail in [15,29], so here we will only briefly present its basic assumptions. An SMA representative volume consists of grains characterized by the orientation ω of the crystallographic axes relative to the selected laboratory basis. The grains consist of a high-temperature phase austenite and orientation variants of martensite formed from austenite by one of *N* crystallographically equivalent variants of transformation of the crystal lattice. The internal variables Φ_n are such that the volume fraction of the *n*-th variant of martensite equals Reuss' averaging scheme is used, so that the strain of a representative volume is calculated by averaging the strains over all grains. The strain of a grain is found as the sum of elastic, thermal, phase, and micro-plastic deformation associated with accommodation of martensite. Active plastic deformation is not taken into account in this work. Elastic and thermal strain of austenite martensite variants are calculated with the Duhamel-Neumann law. The phase strain of the *n*-th variant of martensite is proportional to the Bain strain D_n realizing the transformation of the crystal lattice and to the volume fraction of the *n*-th martensitic variant. Due to the Reuss' hypothesis, the phase strain of the grain is calculated by averaging the phase strains over all orientational variants of martensite:

$$\varepsilon^{gr\,Ph} = \frac{1}{N}\sum_{n=1}^{N} \Phi_n D_n. \quad (1)$$

For calculation of the micro-plastic strain another set of internal variables ε_n^{mp} , that are related to martensitic variants, are introduced. It is assumed that the micro-plastic strain of the grain can be calculated by the relation similar to Eq. (1):

$$\varepsilon^{gr\,mp} = \frac{1}{N}\sum_{n=1}^{N} \kappa\varepsilon_n^{mp}\mathrm{dev}(D_n), \quad (2)$$

where κ is the scaling factor (the material constant), "dev" means the deviator.

Constitutive equations for calculation the evolution of variables Φ_n and ε_n^{mp} are formulated in terms of thermodynamic forces that are the derivatives of the Gibbs thermodynamic potential *G* with respect to these variables. These equations are described in detail in [29].

The condition for the martensitic transformation expresses the equality of the thermodynamic driving force $F_n = -\frac{\partial G}{\partial \Phi_n}$ to some dissipative force F^{fr} caused by the resistance to the growth of martensitic crystals and responsible for the existence of the transformation hysteresis:

$$F_n = \pm F^{fr}, \quad (3)$$

where a sign "+" is taken for the direct and "–" for the reverse transformation. The material constant F^{fr} is calculated through the values of the characteristic temperatures and latent heat of the transformation. When the driving force changes due to variation of temperature and stress, increments of internal variables also change so that condition (3) remains satisfied.

Modeling of pseudo-elastic effect at different strain rates

Simulation of loading and unloading of the cylindrical specimen made of a NiTi SMA at temperature 290 K, when the alloy demonstrates pseudo-elastic behavior, was performed. According to the experimental procedure presented in [20], the cylinder radius is 2.5 mm, the strain rate varied from $3.3\cdot10^{-4}$ to $3.3\cdot10^{-2}$ s^{-1}, maximum value of achieved

strain is 9 %. Material constants for SMA and characteristics of the vibrating system are presented in Table 1.

Table 1. Material constants used for modeling

Material constant	Value
Characteristic temperatures *Mf*, *Ms*, *As*, *Af*, K	224, 227, 262, 265
Latent heat q_0, MJ/m^3	-150
Number of martensite variants *N*	12
Lattice deformation matrix *D*	$\begin{pmatrix} 0.025 & 0.059 & 0.0456 \\ 0.059 & 0.025 & 0.0456 \\ 0.0456 & 0.0456 & -0.042 \end{pmatrix}$
Elastic modulus of austenite E_A, GPa	80
Elastic modulus of martensite E_M, GPa	25
Poisson's ratio of austenite ν_A	0.33
Poisson's ratio of martensite ν_M	0.45
Density of austenite ρ_A, density of martensite ρ_M ,kg/m^3	6500
Thermal-expansion coefficient of martensite, K^{-1}	$6.6 \cdot 10^{-6}$
Specific heat of austenite C_A, J/(kg K)	550
Specific heat of austenite C_M, J/(kg K)	500

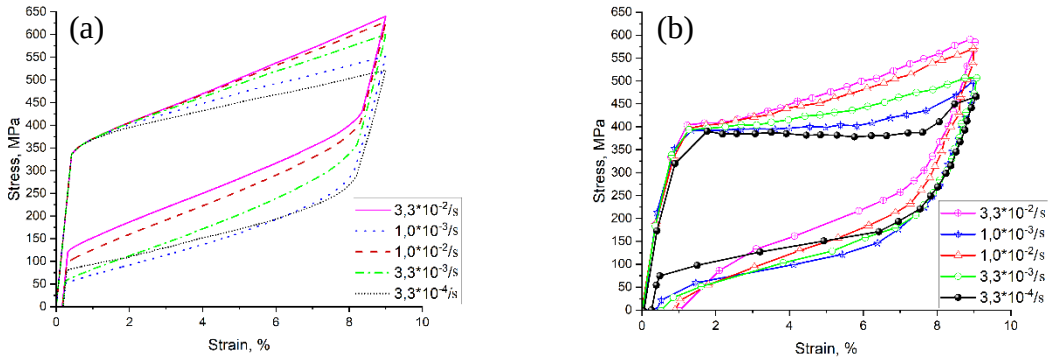

Fig. 1. Stress-strain diagrams for tension of SMA rod at different strain rates: (a) modeling with the microstructural model, (b) experiment [30]

In the first set of numerical experiments it is assumed for simplicity that the temperature in the SMA rod is uniform and the heat exchange is carried out through its surface in accordance with Newton's law. In this case one can write the thermal balance equation:

$$-(\rho_M \Phi_M + \rho_A(1-\Phi_M))(C_M \Phi_M + C_A(1-\Phi_M))\dot{T} + h_{conv}\frac{A_{SMA}}{V_{SMA}}(T - T_{amb}) = q_0 \dot{\Phi}_M, \qquad (4)$$

where ρ_M, ρ_A are the densities and C_M, C_A are the specific heats of martensite and austenite; Φ_M is the total volume fraction of martensite, T_{amb} is the ambient temperature, h_{conv} is the heat transfer coefficient, A_{SMA} and V_{SMA} are the area and volume of the SMA cylinder, dot means the time derivative. The value of h_{conv} was chosen as 80 W/(m^2 K) to be corresponding to a metal-air heat exchange [31].

The calculated stress-strain diagrams and the experimental results of Kan et al. [20] are presented on Fig. 1. One can see good agreement between the model curves and the experimental data. Deformation at higher strain rates causes greater heating of the specimen due to the release of latent heat of the direct martensitic transformation. This leads to increase of the maximum stress while the value of the phase yield limit (stress

at which the elastic mechanism of deformation gives way to a phase one) does not change. As a result, the slope of the pseudo-elastic "flag" becomes steeper.

During unloading such a direct connection between the strain rate and cooling due to the reverse martensitic transformation is not observed. At a high strain rate, the sample does not have time to cool much more than the initial temperature. At a very slow strain rate, the sample does not cool much due to slow heat exchange with the environment. When the strain rate belongs to some medium range, the model specimen manages to cool down due to heat absorption caused by the endothermal reverse martensitic transformation.

Coupled boundary value problem

The results described in the previous section can be considered as the results of solving zero-dimension boundary value problem for the cylinder with the uniform temperature field. This seems acceptable for relatively thin samples and for characteristic deformation duration that assume temperature equalization along the radius of the cylinder. Otherwise, to calculate the deformation of the rod and distribution of temperature along the radius it is necessary to solve a connected boundary-value thermomechanical problem that takes into account heat exchange with the environment, thermal conductivity, the release of latent heat of transformation and the dependence of the change in phase state and deformation on the temperature and stress.

The cylindrical model element of the radius *R* that is in thermal contact with the environment has been considered. An axial force *F* acting along the axis *z* is supposed to be applied to the end of the cylinder (Fig. 2).

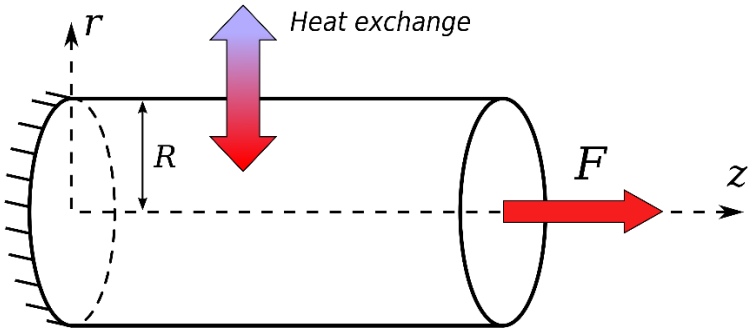

Fig. 2. Tension of a cylindrical rod, which is in thermal contact with the environment through the side surface (scheme)

It was assumed, that the cylinder was long enough so that the peculiarities of the force distribution at the end could be neglected and the cross-sections could be considered to remain flat. As a result, the longitudinal fibers' strain $\varepsilon_{zz} = \varepsilon$ does not depend on the radial coordinate *r*. In the cylindrical coordinate system *r*, φ, *z* non-zero can be strain components $\varepsilon_{rr}(r)$ and $\varepsilon_{\varphi\varphi}(r)$.

Conditions of static equilibrium of a rod under consideration are:

$$\int_S \sigma_{zz} dS = F, \quad (5)$$

where the integration is carried out over the entire cross section of the cylinder.

Let us assume that the constitutive relations of the material allow us to additively divide the total strain ε into elastic ε^{el} and non-elastic ε^{ne}components, so that $\varepsilon = \varepsilon^{el} + \varepsilon^{ne}$. Then, according to Hooke's law:

$$\sigma = E(\varepsilon - \varepsilon^{ne}), \quad (6)$$

where E is the effective Young's modulus, determined in this work by the "mixture rule" for elastic compliances:

$$E^{-1} = \Phi_M E_M^{-1} + (1 - \Phi_M) E_A^{-1}. \quad (7)$$

Increments of phase strain and internal variables were determined by the microstructural model described in the previous section. Formally, they can be written as:

$$\begin{aligned} \Delta\varepsilon^{ne}(r) &= F_1\big(\Delta T(r), \Delta\sigma(r), X(r)\big), \\ \Delta X(r) &= F_2\big(\Delta T(r), \Delta\sigma(r), X(r)\big), \end{aligned} \quad (8)$$

where the functions F_1 and F_2 are determined by the microstructural model and the symbol X denotes the set of internal variables $\Phi_n(\omega)$ and $\varepsilon_n^{mp}(\omega)$ for each of the n variants in each grain ω, correspondingly.

The variation of temperature over time was calculated by solving the heat conduction equation:

$$c\rho\frac{\partial T}{\partial t} = \frac{\partial}{\partial r}\left(\lambda\frac{\partial T}{\partial y}\right) + \dot{Q}, \quad (9)$$

where c is the specific heat capacity, ρ is the density and λ is the thermal conductivity. All these parameters were determined for mixture of martensite and austenite by the same way as it was previously done for the effective elastic compliance (7). The intensity of heat sources is determined by the latent heat of transformation of an SMA q_0 and the growth rate of the total volume fraction of martensite Φ_{M}, so that $\dot{Q} = -q_0\dot{\Phi}_{\mathrm{M}}$.

It is assumed, that heat exchange with the environment occurs according to Newton's law:

$$\mp\ \lambda\frac{\partial T}{\partial y}\Big|_{y=\pm\frac{h}{2}} = h_{conv}(T - T_{env}), \quad (10)$$

where h_{conv} is the heat transfer coefficient, T_{env} is the ambient temperature.

To solve the axis-symmetric problem, a discrete scheme was used. The radius R of the cylinder was divided into K equal segments, thereby determining the nodes of the spatial grid with coordinates $r_j = jR/K,\ j = 1, \ldots K$. The stress, deformation and temperature fields at different points of the body were specified as a set of values at the grid nodes. During the calculation, at each loading step, the problem is divided into sub-problems with their own operators:

1. the mechanical equilibrium problem (an operator $\bar{M}$) – finding of the grid function $\sigma(r)$ for a given value of the applied force F and values $\varepsilon^{ne}(r_j)$ of inelastic deformation at the nodes using relations (5)–(7);
2. the "rheological" problem of finding inelastic deformation and density of heat sources (as well as internal variables) using the microstructural model (8) (an operator $\bar{F}$);
3. the thermal (heat diffusion) problem (an operator $\bar{T}$) – finding of the grid function $T(r_j)$ using the heat conductivity Eq. (9) under given heat exchange conditions (10) and known internal variables.

The search for such stress and temperature fields that satisfied simultaneously equations of equilibrium, thermal conductivity and boundary conditions changing during the step can be reduced to the problem of a fixed point of the operator $\bar{A}$:

$$\begin{pmatrix}\sigma(y)\\ T(y)\end{pmatrix} = \bar{A}\begin{pmatrix}\sigma(y)\\ T(y)\end{pmatrix}. \tag{11}$$

Here the operator $\bar{A}$ is a composition of operators $\bar{M}$, $\bar{F}$ and $\bar{T}$:

$$\begin{pmatrix}\sigma(r)\\ T(r)\end{pmatrix} = \begin{pmatrix}\bar{M}\left(\varepsilon^{ne}(r)\right)\\ \bar{T}\left(\dot{Q}(r)\right)\end{pmatrix}, \qquad \begin{pmatrix}\varepsilon^{ne}(r)\\ \dot{Q}(r)\end{pmatrix} = \bar{F}\begin{pmatrix}\sigma(r)\\ T(r)\end{pmatrix}. \tag{12}$$

In this work, this problem was solved by reducing it to finding the minimum of a functional of many variables [32]. The result of the solution were grid functions for stress, strain, temperature and internal variables of the microstructural model.

Boundary value problem: simulation of pseudo-elastic effect at different strain rates

The computational experiments described in the previous section were carried out by solving of the boundary value problem. The calculated stress-strain diagrams for a cylindrical sample with the radius 2.5 mm are presented on Fig. 3.

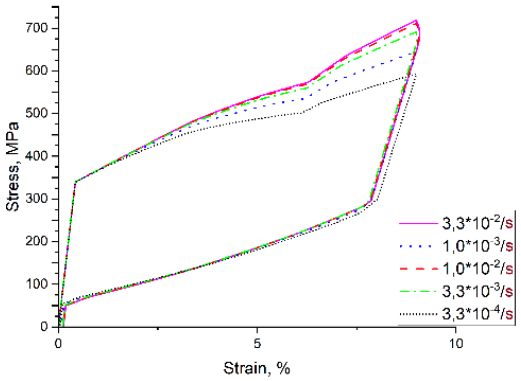

Fig. 3. Stress-strain diagrams for tension of SMA rod at different strain rates – calculated by solving coupled boundary-value problems

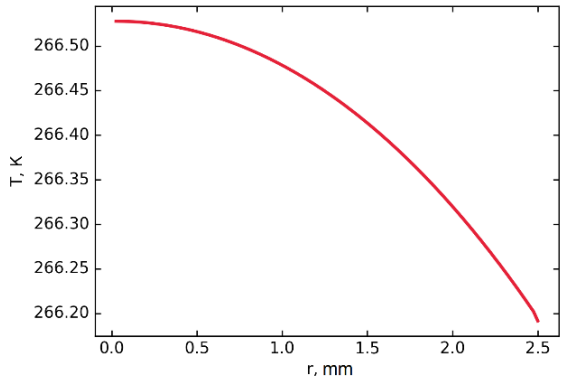

Fig. 4. Temperature distributions along the cylinder radius during deformation up to 9 % at strain rate $3.3{\cdot}10^{-2}$ s^{-1} at the end point of deformation

Although there are some peculiarities on the stress-strain curves in comparison with ones from Fig. 1(a), we can conclude that they are in a good qualitative and quantitative agreement with the results obtained previously. Apparently, at given deformation rates and heat exchange conditions, the temperature field in the sample under consideration does not differ much from the uniform one. The calculation results confirm this fact. Figure 4 shows the temperature distribution along the radius of the sample when the deformation achieved its maximum value of 9 % for the strain rate $3.3{\cdot}10^{-2}$ s^{-1}. The temperature difference in the center and on the surface does not exceed 0.3 K. The less deformation rate, the smaller is this difference.

Criteria for the need to solve the heat conduction equation

Considering the difficulties arising at solving coupled boundary value problems for SMA, the question emerges when it is possible to consider the temperature field to be uniform at given material constants, deformation rate and heat exchange conditions, and thus to avoid solving the heat conduction equation.

To calculate thermal conductivity in non-stationary modes, the Fourier and Biot criteria (numbers) are most often used. Initially, they were formulated for problems that did not imply the presence of internal heat sources. However, at present they are successfully used, for example, for calculating fuel rods of nuclear power plants [33].

The Biot number is the ratio of the internal thermal resistance of a body R/λ (a cylinder with the radius R in our case) to the external thermal resistance (resistance to heat transfer) $1/h_{conv}$:

$$Bi = \frac{h_{conv}R}{\lambda}. \quad (13)$$

This ratio indicates whether the temperature inside a body varies significantly in space when the body is heated or cooled over time by a heat flux at its surface. If the Biot number is small (much smaller than 1), the temperature field inside the body can be considered as nearly uniform. Requiring that Bi must not exceed 0.1, we obtain, for the material parameters presented in Table 1, that $R \leq 12.5$ mm. Therefore, the cylinder under consideration with the radius 2.5 mm satisfies this condition. The Biot number for this radius is 0.02.

The Fourier number characterizes the relationship between the rate of change of thermal conditions in the environment and the rate of redistributing of the temperature field inside the body under consideration. It depends on the characteristic size L of the body and its thermal diffusivity $\chi = \lambda/(\rho C)$:

$$Fo = \frac{\chi t_c}{L^2}, \quad (14)$$

where t_c is the characteristic time of change of external conditions. If we take the total deformation time to a given strain of 9 % as the characteristic time of the process, then for $L = R = 2.5$ mm and the strain rate $3.3 \cdot 10^{-2}$ s^{-1} we obtain $t_c \approx 2{,}7$ s and $Fo \approx 1{,}5$. It is known, that for the Fourier number significantly greater than 1.0 it can be assumed that there is enough time to establish the uniform temperature field across the entire characteristic length of the specimen.

Of course, 1.5 is not much greater than 1.0, nevertheless the model sample shows rather uniform temperature field at the chosen strain rate (Fig. 4). This may be due to the choice of the characteristic time for the characteristic length of the process.

One can try to evaluate the characteristic time and the Fourier number directly from the solution of the boundary value problem of heat conduction theory in dimensionless form with boundary conditions of the third kind. It is known [33] that application of the Fourier method gives the following solution for the cylinder:

$$\theta(x, Fo) = \theta_0 \cdot \sum_{k=1}^{\infty} A_k J_0(\mu_k x) \exp(-\mu_k^2 Fo), \quad (15)$$

$$A_k = \frac{2\, J_1(\mu_k)}{\mu_k \cdot \left(J_0^2(\mu_k) + J_1^2(\mu_k)\right)}, \quad (16)$$

where $x = r/R$ is dimensionless coordinate, $\theta(x, \tau) = T(x, t) - T_{amb}$ is the relative dimensionless temperature at time instant t, $\theta_0 = T_0 - T_{amb}$ is the relative dimensionless temperature at the initial moment of time, μ_k are positive roots of the equation:

$$\mu_k J_1(\mu_k) = Bi\, J_0(\mu_k), \quad (17)$$

(in ascending order). Here $J_\nu(x)$ are Bessel functions of the 1st kind of order *v*.

Keeping only the first term of the series in Eq. (15) one can obtain for the cylinder

$$\theta(x, Fo) = \theta_0 A_1 J_0(\mu_1 x) \exp(-\mu_1^2 Fo), \quad (18)$$

$$A_1 = \frac{2Bi}{Bi^2+\mu_1^2}. \quad (19)$$

Assuming that the permitted temperature difference on the surface (x = 1) and in the center (x = 0) is 1 K, for a given Bi = 0.02 it is possible to estimate the characteristic time. It occurred to be equal about 12 s. The corresponding $Fo \approx 8$ satisfies the condition of uniform temperature distribution. The values of the characteristic times and Fourier numbers for some other radii *R* are given in Table 2.

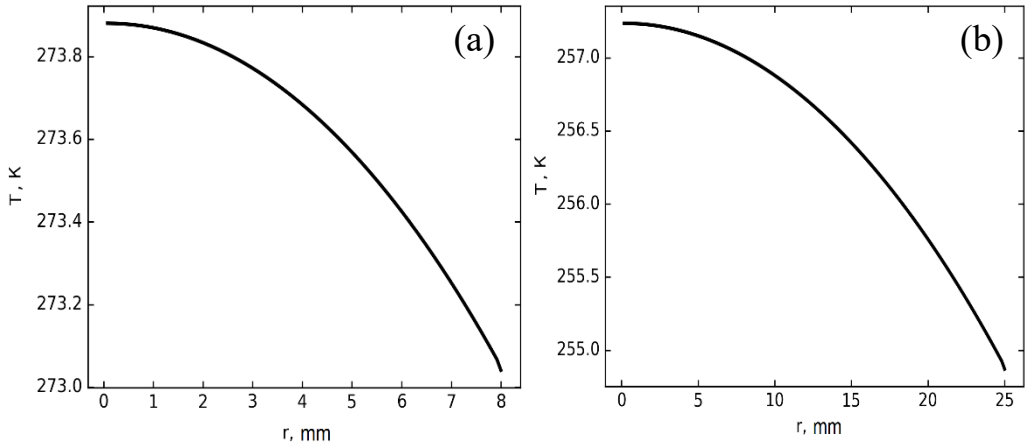

Fig. 5. Temperature distribution along the cylinder radius for R = 8 mm (a), R = 25 mm (b) at the final point of deformation. The strain rate $3.3 \cdot 10^{-2}$ s^{-1}

Figure 5 shows the calculated temperature distributing along the radius for R = 8 mm and R = 25 mm when the strain was 9 %. The maximum temperature difference in the center and on the surface of the sample ΔT in the first case was 0.8 K and in the second 2 K. The results for different radii are also presented in Table 2. One can note that for the permissible value ΔT = 1 K for the given strain rate and heat exchange conditions, the radius should not exceed 8 mm. This value seems to be quite large but although the strain rate $3.3 \cdot 10^{-2}$ s^{-1} is not extremely high, the deformation process takes only 2.7 s and the rod does not have enough time to cool significantly due to heat exchange with the environment.

Table 2. Characteristic times, Fourier numbers and maximum temperature difference

R, mm	2.5	3.0	8.0	9.0	25.0
t_c, s	12	15	49	–	259
Fo	8.0	5.5	2.5	2.3	1.4
ΔT, *K*	0.2	0.3	0.8	1	2

It should also be noted that the temperature fields obtained by solving the connected boundary value problem taking into account heat release and heat absorption demonstrates fairly good agreement with simple evaluations obtained using Fourier and Biot numbers excluding these processes.

Conclusions

1. The microstructural model, taking into account the release and absorption of the latent heat of martensitic transformations, is an adequate tool for describing the strain rate dependence of the pseudo-elastic behavior for SMAs. The strain rate growth forces an increase in the maximum achieved stress and the slope of the pseudo-elastic "flag". The obtained results are in good agreement with the available experimental data.
2. The microstructural model allows solving the boundary value problem of tension of an SMA cylinder in a fully coupled thermomechanical formulation, taking into account the heat exchange with the environment, the release of latent heat of transformation and thermal conductivity. It allowed simulating the pseudo-elastic stress-strain diagrams for different strain rates.
3. The Fourier and Biot criteria can be used to evaluate the critical radius of the cylinder for which, at a given strain rate and given heat exchange conditions, it is necessary to solve a fully coupled boundary value problem taking into account the thermal conductivity of the sample. The obtained estimates were confirmed by solving boundary value problems for cylinders of different radii.

References

1. Duerig TW, Melton KN, Stöckel D. (eds.) *Engineering Aspects of Shape Memory Alloys*. Butterworth-Heinemann; 1990.
2. Wanhill RJH, Ashok B. Shape Memory Alloys (SMAs) for Aerospace Applications. In: Prasad N, Wanhill R. (eds.) *Aerospace Materials and Material Technologies*. Singapore: Springer; 2017.
3. Tabrizikahou A, Kuczma M, Łasecka-Plura M, Farsangi EN, Noori M, Gardoni P, Li S. Application and modelling of Shape-Memory Alloys for structural vibration control: State-of-the-art review. *Constr. Build. Mater.* 2022;342(B): 127975.
4. Zhang W, Zhang Y, Zheng G, Zhang R, Wang Y. A Biomechanical Research of Growth Control of Spine by Shape Memory Alloy Staples. In: *BioMed Research International*. 2013. p.384894.
5. Petrini L, Bertini A, Berti F, Pennati G, Migliavacca F. The role of inelastic deformations in the mechanical response of endovascular shape memory alloy devices. *J. of Engineering in Medicine*. 2017;231(5): 391–404.
6. Otsuka K, Wayman CM. (eds.) *Shape memory materials*. Cambridge: Cambridge University Press; 1998.
7. Pieczyska EA, Tobushi H, Kulasinski K. Development of transformation bands in TiNi SMA for various stress and strain rates studied by a fast and sensitive infrared camera. *Smart Mater. Struct.* 2013;22: 035007.
8. Kato H. Latent heat storage capacity of NiTi shape memory alloy. *J. Mater. Sci.* 2021;56(13): 8243–8250.
9. Louia F, Michaelis N, Schütze A, Seelecke S, Motzki P. A unified approach to thermo-mechano-caloric characterization of elastocaloric materials. *J. Phys. Energy*. 2023:5(4): 045014.
10. He YJ, Sun QP. Frequency-dependent temperature evolution in NiTi shape memory alloy under cyclic loading. *Smart Mater. Struct.* 2010;19(11): 115014.
11. Yin H, He Y, Sun Q. Effect of deformation frequency on temperature and stress oscillations in cyclic phase transition of NiTi shape memory alloy. *J. Mech. Phys. Solids*. 2014;67: 100–128.
12. McCormick P, Liu Y, Miyazaki S. Intrinsic thermal-mechanical behaviour associated with the stress-induced martensitic transformation in NiTi. *Mater. Sci. Eng.: A*. 1993;167(1-2): 51–56.
13. Qiu C, Gong Z, Peng C, Li H. Seismic vibration control of an innovative self-centering damper using confined SMA core. *Smart Struct. Syst., Int. J.* 2020;25(2): 241–254.
14. Jin F, Zhao C, Xu P, Lin J. Nonlinear vibration of SMA hybrid composite beams actuated by embedded pre-stretched SMA wires with tension-bending coupling effect. *J. Sound Vib.* 2024;568: 117964.
15. Vukolov EA, Volkov AE, Evard ME, Belyaev FS. Simulation of bending for a shape memory alloy plate accounting influence of latent heat of transformation and heat exchange with an environment. *Mechanics of Composite Materials and Structures*. 2024;30(2): 198–221. (In-Russian)
16. Brinson L. One-dimensional constitutive behavior of shape memory alloys: Thermomechanical derivation with non-constant material functions and redefined martensite internal variable. *J. Intel. Mater. Syst. Struct.* 1993;4(2): 229–242.
17. Qidwai MA, Lagoudas DC. Numerical implementation of a shape memory alloy thermomechanical constitutive model using return mapping algorithms. *Int. J. Num. Methods in Engineering*. 2000;47(6): 1123–1168.

18. Boyd J, Lagoudas DC. A thermodynamical constitutive model for shape memory materials. Part I. The monolithic shape memory alloy. *Int. J. Plast.* 1996;12(6): 805–842.
19. Panico M, Brinson L. A three-dimensional phenomenological model for martensite reorientation in shape memory alloys. *J. Mech. Phys. Solids.* 2007;55(11): 2491–2511.
20. Chemisky Y, Duval A, Patoor E, Zineb TB. Constitutive model for shape memory alloys including phase transformation, martensitic reorientation and twins accommodation. *Mech. Mater.* 2011;43(7): 361–376.
21. Patoor E, Lagoudas DC, Entchev PB, Brinson LC, Gao X. Shape memory alloys, part I: General properties and modeling of single crystals. *Mech. Mater.* 2006;38(5–6): 391–429.
22. Oliveira SA, Savi MA, Kalamkarov AL. A three-dimensional constitutive model for shape memory alloys. *Arch. Appl. Mech.* 2010;80(10): 1163–1175.
23. Auricchio F, Bonetti E, Scalet G, Ubertini F. Theoretical and numerical modeling of shape memory alloys accounting for multiple phase transformations and martensite reorientation. *Int. J. Plast.* 2014;59: 30–54.
24. Patoor E, Eberhardt A, Berveiller M. Micromechanical modelling of superelasticity in shape memory alloys. *J. de Physique IV, C1.* 1996;6: 277–292.
25. Sun QP, Lexcellent C. On the unified micromechanics constitutive description of one-way and two-way shape memory effects. *J. de Physique IV, C1.* 1996;6: 367–375.
26. Huang M, Brinson LC. A multivariant model for single crystal shape memory alloy behavior. *J. Mech. Phys. Solids.* 1998;46(8): 1379–1409.
27. Volkov AE, Kukhareva AS. Calculation of the stress-strain state of a TiNi cylinder subjected to cooling under axial force and unloading. *Bulletin of the Russian Academy of Sciences: Physics.* 2008;72(9): 1267–1270.
28. Kukhareva A, Kozminskaia O, Volkov A. Calculation of the transformation plasticity strain in the shape memory cylinder. *E3S Web of Conferences.* 2020;157: 06016.
29. Volkov AE, Evard ME, Volkova NA, Vukolov EA. Microstructural modeling of a TiNi beam bending. *Materials Physics and Mechanics.* 2023;51(2): 177–186.
30. Kan Q, Yu C, Kang G, Li J, Yan W. Experimental observations on rate-dependent cyclic deformation of super-elastic NiTi shape memory alloy. *Mechanics of Materials.* 2016;97: 48–58.
31. Belyaev FS, Evard ME., Volkov AE, Starodubova MS. Modeling of vibration protection by shape memory alloy parts with an account of latent heat. *Smart Structures and Systems.* 2024;33(3): 243–251.
32. Ortega JM, Rheinboldt WC. *Iterative Solution of Nonlinear Equations in Several Variables.* Academic Press; 2014.
33. Lienhard JHV, Lienhard JHIV. *A Heat Transfer Textbook.* 5th ed. Cambridge MA: Phlogiston Press; 2020.

About Authors

Fedor S. Belyaev
Candidate of Physical and Mathematical Sciences
Senior Researcher (St. Petersburg State University, St. Petersburg, Russia); Senior Researcher (Institute for Problems in Mechanical Engineering of the Russian Academy of Sciences, St. Petersburg, Russia)

Aleksandr E. Volkov
Doctor of Physical and Mathematical Sciences
Professor (St. Petersburg State University, St. Petersburg, Russia)

Egor A. Vukolov
PhD Student (St. Petersburg State University, St. Petersburg, Russia)

Margarita E. Evard
Candidate of Physical and Mathematical Sciences
Associate Professor (St. Petersburg State University, St. Petersburg, Russia)

Kristina V. Kudrina
Student (St. Petersburg State University, St. Petersburg, Russia)

Mariya S. Starodubova
Student (St. Petersburg State University, St. Petersburg, Russia)